# Reverse Engineering and Core Loss Quantification in an Industrial Synchronous Reluctance Motor Drive


Balša Ćeranić
*School of Electrical Engineering*
*University of Belgrade*
11120 Belgrade, Serbia
ceranic@etf.bg.ac.rs

Leposava Ristić
*School of Electrical Engineering*
*University of Belgrade*
11120 Belgrade, Serbia
leposava.ristic@etf.bg.ac.rs

Mladen Terzić
*School of Electrical Engineering*
*University of Belgrade*
11120 Belgrade, Serbia
terzic@etf.bg.ac.rs

Milan Bebić
*School of Electrical Engineering*
*University of Belgrade*
11210 Belgrade, Serbia
bebic@etf.bg.ac.rs



***Abstract*—Synchronous Reluctance Motors (SynRMs) are considered to be a more efficient alternative to Induction motors (IMs) and a cheaper alternative to Permanent Magnet Synchronous Motors (PMSMs). The aim of this work is to apply reverse engineering procedure on an existing machine and create a precise model for finite element analysis (FEA) that can further be used for co-simulation with a separate simulation of control algorithm. This model is then used to quantify core losses in this machine via FEA. Power loss measurements were also collected from an experimental setup and analytical calculations were used to extract iron core loss information and compare the two sets of results.**



***Keywords—Synchronous reluctance motor, iron core losses, reverse engineering, finite element analysis, drive***


## I. Introduction

Electrical drives are responsible for over 53% of globally consumed electrical energy [1], of which around 60% is produced from fossil fuels [2]. Sine fossil fuel usage leads to emission of harmful gasses, the international community's efforts to curb global warming call for a thorough reassessment of energy efficiency in electrical drives [3]. Efficiency of electrical motors is an important factor in overall drive efficiency, and it can be increased by choosing different machine design and control algorithms.

The Synchronous Reluctance Motor (SynRM) has recently garnered significant attention, being promoted as a more efficient alternative to Induction Motors (IMs) when employing appropriate control algorithms [17] and a more cost-effective and environmentally friendly alternative to Permanent Magnet Synchronous Motors (PMSMs) [18]. This modern and energy efficient motor type was selected to showcase reverse engineering procedure for electrical machines, resulting in a high precision model of the physical device.

Results of reverse engineering can be used in different purposes. From the aspect of motor design, it can help improve design by identifying limitations and weaknesses in existing machines. The model created by reverse engineering can be imported into a simulation environment and tested to refine control algorithms and improve overall drive efficiency, all without access to original design documentation.

In this work, motor model was developed using finite element analysis, and is used in offline simulations to evaluate iron core losses in different operation modes. Simulations were based on a FEM analysis that considers effects of the machine's geometry on magnetic field distribution and core losses.

After presenting the theoretical basis for SynRMs, creation of this FEM model via reverse engineering is described in Section 2. Results of reverse engineering, i.e. motor parameters, were evaluated using an analytical approximation of inductances. Finally, the simulation for determining core losses is presented. Section 3 shows the simulation results, alongside analytics-enhanced experimental results and offers a comparison. In Section 4, appropriate conclusions are drawn.

## II. Model and Reverse Engineering of SynRM

When alternating current in the stator winding of SynRM generates magnetic field in the core along the stator *d*-axis ($d_s$), motor's magnetically anisotropic rotor tends to assume the position of maximum inductance (minimum magnetic reluctance) relative to the generated magnetic field, thus creating reluctant torque. Whole of the synchronous reluctance motor's torque originates from reluctant torque. [4].

### A. Mathematical model of SynRM

The equivalent circuits in *dq* reference frame for steady states, used for SynRM analysis are presented in Figure 1[5].

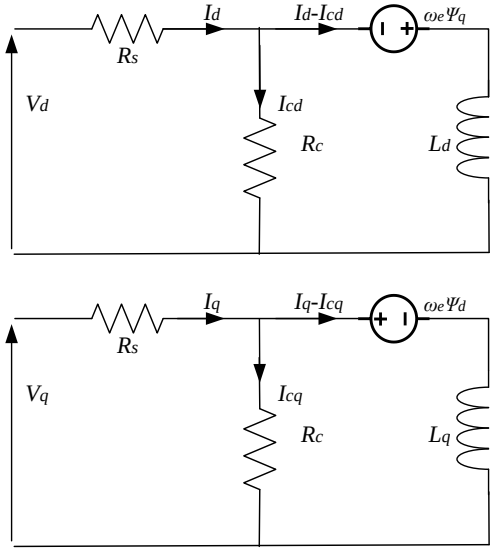


Figure 1: Equivalent circuits of SynRM in *d*-axis(above) and *q*-axis(below)


This is the authors' accepted manuscript of a paper published in Proceedings of 9th International Conference on Environment-Friendly Energies and Applications (EFEA 2025)
The final version of record is available via IEEE Xplore

Parameters in these circuits ($R_s$=1.43Ω, $L_d$=157mH, $L_q$=26mH) were obtained from a parameter identification procedure of frequency converter (ID Run), done on the laboratory setup, while the iron loss resistance $R_c$ is assumed to be 3kΩ. Voltage equations (1) and (2) are derived from equivalent circuit,

$$V_d = R_s I_d - \omega_e \Psi_q \tag{1}$$

$$V_q = R_s I_q + \omega_e \Psi_d, \tag{2}$$

where $u_d, u_q, i_d, i_q$ and $\omega_e$ are: stator voltages in *d*- and *q*- axes, stator current in *d*- and *q*- axes and frequency of rotating field generated by the stator winding. Fluxes in *d*- and *q*- axes are defined in (3) and (4):

$$\Psi_d = L_d(I_d - I_{cd}) \tag{3}$$

$$\Psi_q = L_q(I_q - I_{cq}) \tag{4}$$

Inductances in *d*- and *q*- axes are labeled as $L_d$ and $L_q$, and they do not depend on rotor position if the rotor reference frame is considered [6, 7]. Currents $I_{cd}$ and $I_{cq}$ are currents in the parallel branch, used to model core losses. Copper losses are calculated as in (5) and core losses as in (6).

$$P_{\gamma Cu} = \frac{3}{2} R_s ({I_d}^2 + {I_q}^2) \tag{5}$$

$$P_{\gamma Fe} = \frac{3}{2} R_c ({I_{cd}}^2 + {I_{cq}}^2) \tag{6}$$

This model is completed with torque and flux equations, which are used to calculate $I_d$ and $I_q$ components for the given load torque and flux values.

$$T_e = \frac{3}{2}(L_d - L_q) I_d I_q \tag{7}$$

$$\Psi = \sqrt{(L_d I_d)^2 + (L_q I_q)^2} \tag{8}$$

In this paper, it is assumed that $\Psi$ depends on $T_e$ due to the optimization algorithm employed in the frequency converter, that decreases motor flux reference on lower loads. The function which is recorded at the experimental setup in the laboratory is shown in Figure 2. The authors believe this function corresponds to Maximum Torque per Ampere algorithm, with the value of reference flux limited from below [8].

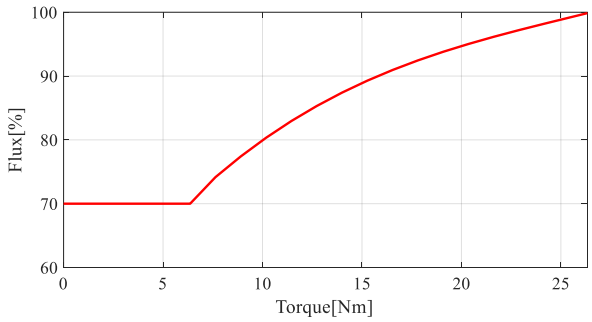


Figure 2: Flux reference dependence on load ($T_{rated}$=25.5Nm), recorded on the experimental setup in the laboratory

By solving equations (7) and (8) with known torque and flux values, $I_d$ and $I_q$ current references are obtained. These currents are used in the reverse-engineering procedure, and later in finite element analyses, for defining the excitation. In order to fully define the excitation, another value that is required is the torque angle δ, which is the angle between rotor *d*-axis and stator current phasor $I_s$. Relation between torque angle δ and torque is given in (9), with *P* denoting the number of pole pairs [9]:

$$T_e = \frac{3P}{2}\frac{1}{2} \cdot (L_d + L_q) \cdot {I_s}^2 \cdot \sin(2\delta) \tag{9}$$

Considering these remarks, sets of current references and power angle can be numerically calculated for different torque values. The data is given in Table I.

TABLE I. CURRENT REFERENCES AND TORQUE ANGLES FOR REQUIRED VALUES OF MOTOR TORQUE

| **Torque [%]** | **$I_d$ reference** | **$I_q$ reference** | **δ** |
|---|---|---|---|
| 0 | 5.53A | 0A | 0º |
| 25 | 5.51A | 2.94A | 28.00º |
| 50 | 6.69A | 4.84A | 35.90º |
| 75 | 7.33A | 6.63A | 42.14º |
| 100 | 7.71A | 8.40A | 42.44º |

### *B. Reverse Engineering of SynRM*

In this section, a procedure of reverse engineering of an electric machine using ANSYS Electronics Desktop software is presented. The aim of this procedure is to determine unknown parameters and dimensions of an existing SynRM [10], based on rated parameters and dimensions that were accessible. Resulting machine design is then used to determine core loss dependencies on motor speed and load torque, using Finite Element Analysis (FEA).

Data used in this procedure, consisting of machine dimensions and geometry characteristics, as well as the rated motor parameters, is given in the Appendix.

Known dimensions and parameters were measured on a motor disassembled for the purpose of re-winding. Stator and rotor diameters, as well as the core length and coil pitch, were easily measured, as well as the rotor barrier dimensions. However, exact slot dimensions were not accessible with the used measuring tools. The number of conductors and their disposition was indistinct and hard to determine without cutting through the wires, so the authors considered those parameters unknown as well.

After creating a new ANSYS RMxprt model of SynRM and inserting all known dimensions, the exact stator slot dimensions needed to be determined. The objective of this phase of reverse engineering was for the magnetic flux density to reach empirical values in the slot tooth (up to 2T) and stator yoke (up to 1.5T). The slot dimensions were successfully tuned using the iterative method.

Afterwards, the obtained geometry was exported in ANSYS Maxwell 2D, software tool for FEA. In this tool, number of conductors was varied in order to determine its exact value that best corresponds to the rated values of RMS value of electromotive force first harmonic, RMS value of magnetic flux,

and electromagnetic torque average. Currents $I_d$ *and* $I_q$ were defined to correspond to experimental values at idle operation, with load torque, consisting of friction of machines being around 13.8%. Phase currents were defined as:

$$i_a(t) = \sqrt{{I_d}^2 + {I_q}^2} \cdot \sin(\omega t - \theta_{offset}) \quad (10)$$

$$i_b(t) = \sqrt{{I_d}^2 + {I_q}^2} \cdot \sin(\omega t - \theta_{offset} - \frac{2\pi}{3}) \quad (11)$$

$$i_c(t) = \sqrt{{I_d}^2 + {I_q}^2} \cdot \sin(\omega t - \theta_{offset} - \frac{4\pi}{3}) \quad (12)$$

where $\theta_{offset}$ takes into consideration the phase shift of the stator current phasor referent to the q-axis. Torque angle is defined as the angle between d-axis and stator current phasor, so the offset is calculated as $\theta_{offset} = tan^{-1}(I_q/I_d) - \pi/2$.

Analytical data was collected from a Simulink simulation of DTC-controlled SynRM.

The closest results that could be achieved are presented in Table II, where number of conductors per section per slot was N=24, and this value was adopted for further analysis.

TABLE II. RESULTS OF REVERSE ENGINEERING PROCEDURE

| Value | FEM-based | Analytical |
|---|---|---|
| Current RMS | 4.373A | 4.382A |
| Flux RMS | 1.118Wb | 0.951Wb |
| Torque average | 3.633Nm | 3.625Nm |
| EMF 1st harmonic RMS | 306.4V | 315.1V |

Final look of the reverse engineered SynRM design is shown in Fig.3.

### C. *Analytical verification of model*

In order to verify the reverse engineered design, an analytical calculation of *dq* inductances was brought forth. For analytical calculations, (13) and (14) were used [11]:

$$X_q = \frac{6\mu_0 Dlf}{p^2 g_q''}\left(k_{w1}N_{ph}\right)^2 + X_\sigma \quad (13)$$

$$X_d = \frac{6\mu_0 Dlf}{p^2 g_d''}\left(k_{w1}N_{ph}\right)^2 + X_\sigma \quad (14)$$

In these equations, $D$=0,104m is the inner perimeter of the stator, $l$=0,35m is the length of the magnetic core, $f$=50Hz is the stator frequency, $p$=2 is number of pole pairs, $g_q''$ and $g_d''$ are effective widths of air gap along the $q$ and $d$ axes, $k_{w1}$ is the winding factor, $N_{ph}$ is the total number of conductors in one phase and $X_\sigma$ is the leakage inductance.

Winding factor is calculated as $k_{w1}$=0,909 in accordance to (15):

$$k_{w1} = \frac{sin\left(\frac{m}{z}\frac{\pi}{2}\right)}{m \cdot sin\left(\frac{\pi}{2z}\right)} sin\left(\frac{y}{z}\frac{\pi}{2}\right)^2, \quad (15)$$

where $z$ is the number of slots per pole, $m$ is the number of slots per pole per phase, and $y$ is the coil pitch. The number of conductors per section per slot is $N_s$=24, so the number of conductors in a phase is $N_{ph} = \frac{36}{3}N_s = 288$.

Leakage reactance is neglected in this approximation, and the unknown effective width of air gap along $q$-axis can be approximated as follows: $q$-axis is orthogonal to the length of the barriers, and the effective airgap width is approximately equal to the sum of average rotor barrier widths, as the barriers represent the dominant source of magnetic resistance.

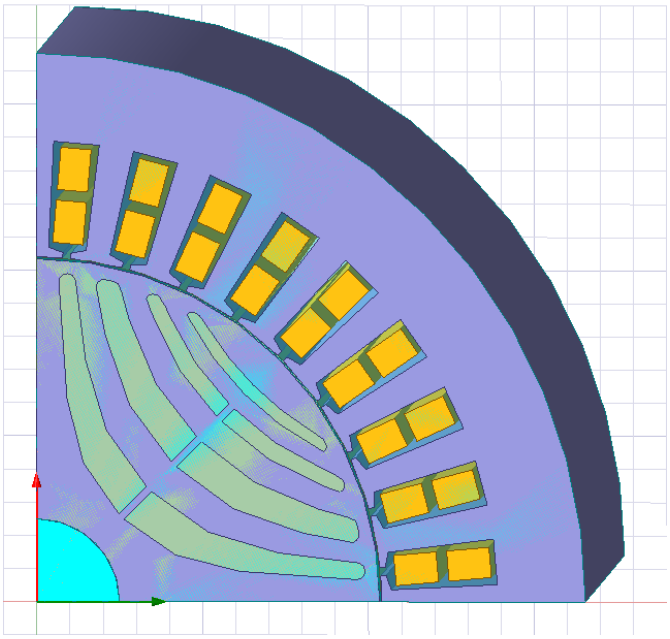

Figure 3: Final SynRM model design in 3D representation

Regarding the $d$-axis effective airgap width, barriers direct the magnetic field through part of the rotor area, and that manifests in increasing the effective air gap. It is approximated that the physical dimensions of the gap between stator and rotor are multiplied by 2 because of barriers, and again by 2 because of slotting. With adopting values of $g_q'' = 10.6$mm and $g_d'' = 1{,}2$mm, the calculations result in inductances given in Table III, where they are listed along with values given by Automatic parameter identification procedure on laboratory setup (ID run). Table III also offers values of stator resistance, both acquired by ID run and calculated using (16):

$$R_{DC} = \frac{l_c}{\sigma_{Cu} S_c}, \quad (16)$$

where $\sigma_{Cu} = 56 \cdot 10^6 \frac{\mathrm{S}}{\mathrm{m}}$ is the conductivity of conductor, $l_c$ total conductor length, and $S_c$ is area of conductor cross section. Wire profile is approximated from the slot dimensions, with respect to fill factor, which is usually around 50%. Resulting area is $S_c = 0{,}8454\mathrm{mm}^2$. This number corresponds to a wire of 1mm in diameter. For calculation of total length of conductor $l_{av}$, the empirical formula (17) was used [12]:

$$l_{av} = 2l + 2.4 \cdot \frac{y\pi(D + H_{slot})}{2\,p\,z} + 0.1 = 0.54\text{m}, \quad (17)$$

where $H_{slot}$ is the slot height, while other values are previously defined. Total length of conductors in phase winding is 288 times greater, so the resistance equals 3.01Ω. This means that the winding is wound in two parallel branches. Regarding the inductance values, while the analytically calculated $L_q$ is similar to the one acquired via the standard ID Run procedure of the converter, analytically calculated value of $L_d$ is significantly greater than the one measured by the frequency converter. This is due to analytical calculations not taking the saturation effects into account.

TABLE III. RESULTS OF ANALYTICAL CALCULATION COMPARED TO VALUES FROM ID RUN PROCEDURE

| | **Analytic** | **ID Run** |
|---|---|---|
| $L_d$ [mH] | 203 | 157 |
| $L_q$ [mH] | 23 | 26 |
| $R_s$ [Ω] | 3.01 | 1.43 |

## III. CORE LOSS QUANTIFICATION

### A. *Finite element analysis*

In order to determine core losses for different motor speeds and loads, transient electromagnetic simulations were run in ANSYS Maxwell 2D software tool. In the simulation model, phase windings were injected with reference phase currents calculated using $I_d$ and $I_q$ current references obtained via analytical calculations. For each steady state, initial position of rotor was set, according to (9), for the purpose of achieving the desired torque values.

Core losses are calculated by the software, using (18), representing Steinmetz's equation with coefficients included in the mathematical model of the chosen material [13],

$$P_{\gamma Fe} = K_h f {B_m}^2 + K_c (f B_m)^2 + K_e (f B_m)^{1.5} \quad (18)$$

where $B_m$ is the amplitude of AC flux component, $f$ is the frequency, and $K_h$, $K_c$ and $K_e$ are hysteresis, eddy-current and excess core loss coefficients, respectively. These coefficients take on the values: $K_h$=172.84, $K_c$=1.37 and $K_e$=1.76.

Before running the FEM simulations, finite element grid needed to be adjusted. Finite element dimension was set to a 5$^{th}$ of the air gap width in the air gap, a 10$^{th}$ of yoke width in the core and three 10$^{th}$s of yoke width in air not including the air gap (slots and barriers).

After running the FEM simulations for speeds of 600, 900, 1200 and 1500 rpm, on several different torque values, close to 0%, 25%, 50%, 75% and 100% of rated torque, losses were determined for each separately defined motor part. In this case, rotor and stator were defined separately, but the core can be divided differently if there is a need for observing losses in smaller parts of the machine. Rotor core losses are presented in function of load torque in figure 4, where different curves represent different speeds, and stator core losses are presented in figure 5, similarly. Iron core loss dependence on motor speed, which is proportional to motor frequency, is shown in Fig.6.

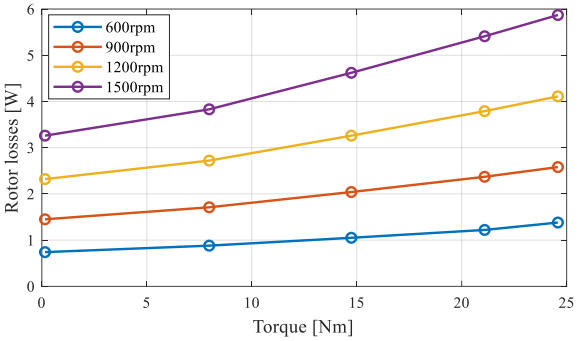


Figure 4: Rotor core loss dependence of torque and speed

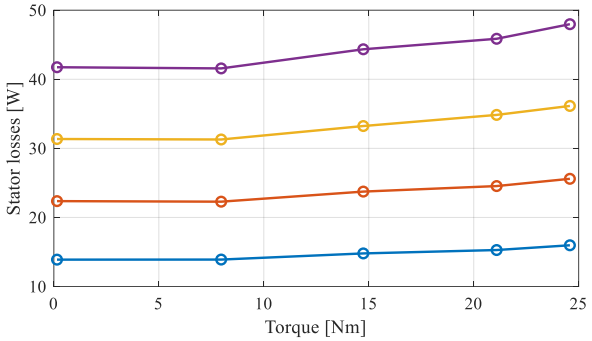


Figure 5: Stator core loss dependence of torque and speed

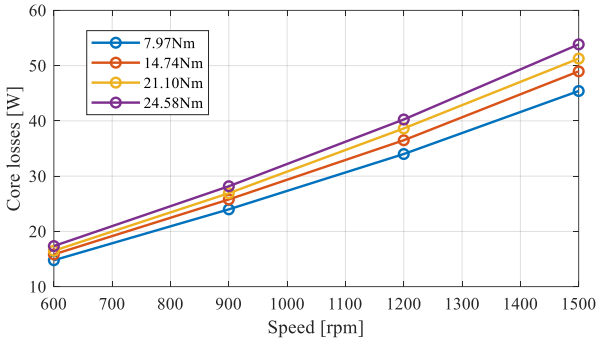


Figure 6: Total core loss dependence on speed, for different motor torque values, determined by FEM simulation

These results correspond to what was expected, hysteresis losses are dominant due to laminated structure of stator and rotor that greatly decreases eddy current losses. This is mirrored in predominantly linear dependence of losses on motor frequency.

Some losses are present in rotor as well, due to spatial harmonics caused by machine slotting, but their values represent a small part of total power losses in the machine.

### B. *Experiment*

Experimental part of the work was done in the Laboratory for Electrical Drives in School of Electrical Engineering, University of Belgrade, purpose of which was to validate the results of previously conducted simulations and obtain a more complete picture of SynRM losses.

The laboratory setup consists of the components shown in Figure 7, that are listed below in the order corresponding to the numbers indicated in the figure.

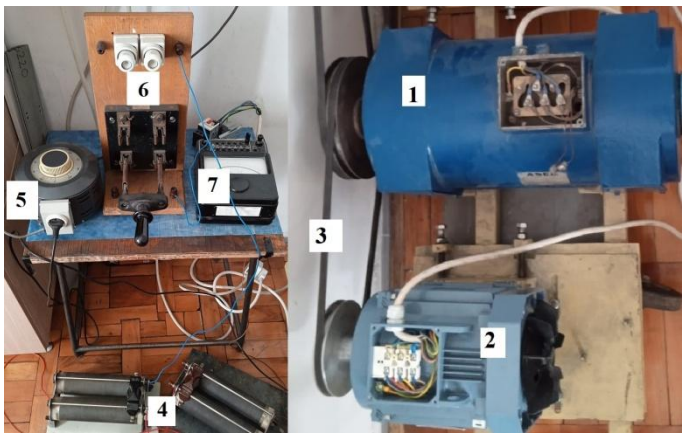


Figure 7: Laboratory setup: 1. ASEA DC motor in dynamic braking mode, used for applying load to the SynRM. Motor data is given in the appendix. 2. ABB Synchronous Reluctance Motor. Motor data is given in the appendix. 3. Belts for mechanical coupling of the motors. 4. Two braking resistors in DC motor circuit, resistance 15Ω. 5. Autotransformer for supplying stator voltage to the field winding of DC motor. 6. Circuit breaker for DC motor rotor circuit. 7. Voltmeter for measuring the field winding voltage.

SynRM in this setup is powered by ABB ACS880-11 frequency converter [14], data of which is given in the appendix. This is a frequency converter with active rectifier that has the capability of powering induction motors, PMSMs and SynRMs. This frequency converter uses Direct Torque Control (DTC) method [15] with optimization algorithm, which the authors believe to be Maximum Torque per Ampere algorithm [8]. This optimization algorithm cannot be overrun, and it dictates the flux reference depending on load torque.

Power, speed and torque measurements were recorded using Drive Composer Entry [16], ABB's software tool for commissioning and maintaining drives with the company's frequency converters. This tool offers measurements of power input into the converter, power output out of the converter, which is equal to the input power of the machine, since the machine is connected with a short cable, and an estimation of motor shaft power.

In order to compare losses from the experiment and FEM analysis, the measurements of the converter are compared to total losses from simulations, which are acquired by adding analytically calculated copper losses (referring to table I for current values) to core losses from the previous subsection.

The experiment consists of providing load to SynRM by adjusting the stator voltage of DC motor in dynamic braking mode. The experiment was conducted on speeds of: 600rpm, 900rpm, 1200rpm and 1500rpm. Higher torques on lower speeds were not possible to achieve, owing to the well known limitation of the dynamical braking mode of DC motor operation.

Values of grid power, motor input power and motor shaft power were measured from the converter. These values are estimated using a certain procedure of the converter manufacturer, and loaded into the software with a resolution of 10W and sampling frequency of 10Hz. Data is extracted in the form of average values over a 2 second interval in steady state operation. Motor losses are calculated as a difference between motor input power and motor shaft power. As it was explained above, winding losses are subtracted from this power difference, result representing pure core losses.

Figure 8 shows total motor losses determined both experimentally (dotted lines) and by analytically-enhanced FEA-based approach (full lines), at speeds of 1200 and 1500rpm. Figure 9 shows the same quantities at speeds of 600rpm and 900rpm.

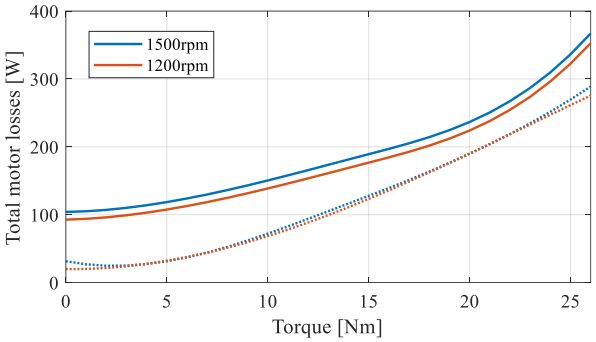


Figure 8: Total power loss dependency of motor torque, on drive speeds of 1200rpm and 1500rpm, determined via FEA (full lines) and experimentally (dotted lines)

The experimental results are rather questionable, as total motor losses estimated by the converter at rated torque and speed are equal to 283W, while only copper losses at rated current are 270W. Main problems of this experiment are uncertainties around estimation method of motor shaft power, as well as low-resolution measurements and a possible hidden optimization algorithm that might be implemented alongside flux optimization.

It should be emphasized that, for speeds of 600rpm and 900rpm, data is incomplete – higher loads could not be reached for lower speeds because of limited DC motor field winding voltage. Highest torque achieved on 600rpm was 14.8Nm and 20.6Nm on 900rpm, and the figure limits correspond to those values.

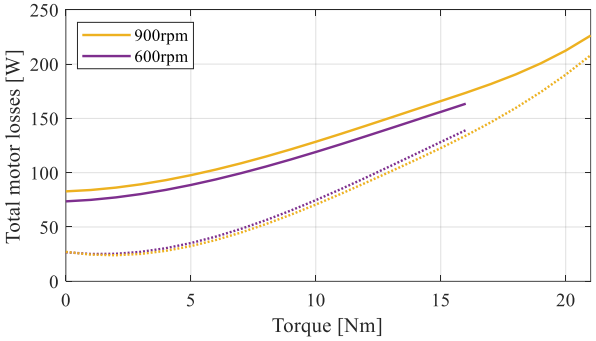


Figure 9: Total power loss dependency of motor torque, on drive speeds of 600rpm and 900rpm, determined via FEA (full lines) and experimentally (dotted lines)

Regarding the difference between these two ways of loss quantification, it is obvious that they are greater in the simulation on FEM model, as it takes into account slot harmonics and more precise flux distribution. Another possible reason for the differences is that the material used in the actual motor has different characteristics than the material adopted in the FEM simulation, and the coefficients included in the model have higher values than those of the material used in the actual machine. This possibility, however, has no effect on the

experimental results, but it is possible that the actual material is of better performances than the one used in the simulation.

## IV. Conclusion

SynRMs are emerging as a more efficient alternative to induction motors, which are currently the most widespread type of electric motors in the industry. They are considered a cheaper and more reliable alternative to PMSMs, which, despite improved efficiency, are accompanied by issues stemming from the use of permanent magnets. For these reasons, researchers are examining the impact of design parameters of SynRMs on performance and are working on developing control algorithms to further improve this motor's capabilities.

This work combines theoretical foundation of this modern machine type, computer simulations and experimental evaluation of theoretical analysis and simulation results of the machine's performance. It includes simulations on a reverse engineered FEM model of a real machine.

Motivation for this work is laid out in the introduction, after which the basic mathematical model of the machine was described. Next, a reverse engineering procedure of a SynRM was performed, where available motor data was used to determine the unknown parameters and to establish the exact motor design. Based on this, a machine model for finite element method analysis was created. Simulations were run on the created model, which resulted in core losses, that cannot be easily and precisely determined analytically or experimentally.

Finally, an experiment was performed, results of which were compared to FEA simulation.

Further research can be directed towards the development of advanced control algorithms for electric drives with SynRMs, by combining FEM model of machine with the control model within the cosimulation.

## Acknowledgment

This work is partially financially supported by the Ministry of Science, Technological Development and Innovation of the Republic of Serbia under contract number: 451-03-137/2025-03/200103 and partially by the European Union's HORIZON – WIDERA – 2021 – ACCESS – 03 under grant agreement No 101079200 (SUNRISE). Also, the equipment used for the research in the Laboratory for Electrical Drives at the School of Electrical Engineering University of Belgrade was provided by the company MIKA Projekt Servis in memory of the late young engineer Radovan Ilić.

## Appendix

TABLE IV. SynRM data from motor plate and catalogue:

| | |
|---|---|
| Rated power | 4kW |
| Rated current | 9.4A |
| Rated line voltage | 380V |
| Rated torque | 25.5Nm |
| Nominal efficiency | 86.6% |
| Overload | 1.5 |
| Motor mass | 27kg |
| Moment of inertia | 0.0069kgm$^2$ |
| Power factor | 0.75 |

TABLE V. DC motor data

| | |
|---|---|
| Rated power | 8.5kW |
| Rated rotor voltage | 410V |
| Rated stator voltage | 220V |
| Rated rotor current | 23.9A |
| Rated stator current | 1.9A |
| Rated speed | 2000rpm |

TABLE VI. SynRM dimensions used in FEM model creation

| | |
|---|---|
| Inner diameter – stator | 104mm |
| Outer diameter – stator | 165.4mm |
| Core length – stator and rotor | 135mm |
| Yoke width | 17.3mm |
| Number of slots | 36 |
| Rotor diameter | 103.4mm |
| Shaft diameter | 35.8mm |
| Core length – rotor | 135mm |

## References

[1] D. de Souza et al, "Life cycle assessment of electric motors – A systematic literature review" *Journal of Cleaner Production*, vol. 456, Elsevier 2024.

[2] H. Ritchie, P. Rosado, *"Electricity Mix"* [Online] Available: https://ourworldindata.org/electricity-mix (10.10.2025)

[3] J. Kim et al, "Energy, material, and resource efficiency for industrial decarbonization:", *Energy Research & Social Science*, vol. 112, Elsevier, 2024.

[4] T. Miller et al, "Design of a Synchronous Reluctance Motor Drive", *IEEE Transactions on Industry Applications*, vol. 27, pp 741-749, 1991.

[5] M. Gecić, *Energy Efficient Digital Control of Permanent Magnet Synchronous Motor in High Speed Region*, PhD Thesis, Faculty of Technical Sciences Novi Sad, 2016

[6] M. Kazmierkowski R. Krishnan, F. Blaabjerg, *Control in power electronics: selected problems*, Academic Press, 2002.

[7] I. Boldea, L. Tutelea, *Reluctance Electric Machines: Design and Control*, CRC Press, 2018.

[8] G. Foo, X. Zhang, "Robust Constant Switching Frequency-Based Field-Weakening Algorithm for Direct Torque Controlled Reluctance Synchronous Motors" *IEEE Transactions on Industrial Informatics*, vol. 12, No. 4, pp 1462-1473 2016.

[9] Ramu Krishnan, *Permanent Magnet Syncronous and Brushless DC Drives*, CRC Press, Sept 2009, ISBN 9780824753849

[10] ABB Technical data, High output synchronous reluctance motors, 1500 r/min, Available: http://www.elbe.it/elbe/contenuti/immagine/5773a2b4-c7db-425d-8201-1715ac12b035 (3.10.2025.)

[11] T. Miller, Brushless permanent-magnet and reluctance motor drives, Oxford University Press, 1989.

[12] J. Pirhonen, T. Jokinen, V. Hrabovcova, Design of rotating electrical machines, Wiley, 2014.

[13] Ansys Electromagnetics Suite, 2023 R1, Maxwell Help, Assigning Materials 10-46, Ansys Inc.

[14] ABB Catalog, ABB industrial drives, ACS880, single drives 0.55 to 3200kW, [Online] Available: https://library.e.abb.com/public/2ea96e5d24c1419794e6f126d537c301/ACS880-PHTC04U-EN_Rev_A.pdf (3.10.2025.)

[15] I. Takahashi, T. Noguchi, "A New Quick-Response and High-Efficiency Contol Strategy of an Induction Motor", *IEEE Transactions on Industry Applications*, vol. 22, 1986.

[16] ABB User's Manual, Drive Composer start-up and maintenance PC tool, [Online] Available: https://library.e.abb.com/public/aaad78b977104094b2c60d9e7191973a/EN_DriveCompPC_tool_UM_Z_A4.pdf (3.10.2025.)

[17] "Experimental Comparison between Induction and Synchronous Reluctance Motor Drives" by M. Villani et al. (2018).

[18] "Permanent Magnet vs Reluctance vs Hysteresis Synchronous Motor: A Comprehensive Comparison," Leili Motor. [Online] Available https://leili-motor.net/permanent-magnet-vs-reluctance-vs-hysteresis-synchronous-motor-a-comprehensive-comparison.html (6.10.2025.)